Spectroscopy of a narrow-line laser-cooling transition in atomic dysprosium

Mingwu Lu, Seo Ho Youn, and Benjamin L. Lev
Department of Physics, University of Illinois at Urbana-Champaign, Urbana, Illinois 61801-3080, USA
(Received 15 September 2010; published 18 January 2011)

The laser cooling and trapping of ultracold neutral dysprosium has been demonstrated recently using the broad, open, 421-nm cycling transition. Narrow-line magneto-optical trapping of Dy on longer wavelength transitions would enable the preparation of ultracold Dy samples suitable for loading optical dipole traps and subsequent evaporative cooling. We have identified the closed 741-nm cycling transition as a candidate for the narrow-line cooling of Dy. We present experimental data on the isotope shifts, the hyperfine constants A and B, and the decay rate of the 741-nm transition. In addition, we report a measurement of the 421-nm transition's linewidth, which agrees with previous measurements. We summarize the laser-cooling characteristics of these transitions as well as other narrow cycling transitions that may prove useful for cooling Dy.

DOI: 10.1103/PhysRevA.83.012510 PACS number(s): 32.70.Cs, 37.10.De

I. INTRODUCTION

Because of its extraordinarily large ground-state magnetic dipole moment (10 bohr magnetons), dysprosium is a prime candidate for the study of ultracold dipolar physics [1]. The Dy atom belongs to the lanthanide (rare-earth) group and has ten $4f$ elections in an open shell submerged under closed s shells. Numerous combinations of valence electron couplings lead to a multitude of electronic energy levels. Laser cooling Dy in a traditional manner would require an impractical number of repumper lasers due to the large number of metastable states below 421 nm (see Fig. 1). Consequently, preparation of cold Dy samples had been limited to the method of buffer gas cooling [4]. Recent progress in the laser cooling and trapping of Dy atoms in a magneto-optical trap (MOT) without a repumper [5] now allows the creation of large population samples with temperatures 500 times colder than those cooled by buffer-gas-cooled. Laser cooling and trapping Dy constitutes an alternative route toward achieving Bose and Fermi degeneracy in this most magnetic of atoms [4].[1]

However, further progress necessitates the optical trapping of Dy [6] so that evaporative cooling may proceed without trap losses arising from dipole-relaxation-induced inelastic collisions [7]. A possible solution lies in the narrow-line cooling of Dy in a manner similar to that demonstrated in the highly magnetic erbium system [8]. A narrow-line Dy MOT could produce Dy temperatures in the microkelvin range. Such ultracold samples would be readily confined in standard optical dipole traps (ODTs).

We focus here on the characteristics of the cycling transition at a wavelength of 741 nm. We believe this transition to be a prime candidate for creating a narrow-line MOT in a manner similar to that demonstrated in Ref. [8] for Er. Existing spectroscopic data [2] are insufficient for implementing the 741-nm narrow-line MOT, and we present here measurements of this transition's hyperfine structure, isotope shifts, and lifetime. Together these measurements provide a sufficient spectroscopic guide for attempting the 741-nm narrow-line cooling of Dy's bosonic and fermionic isotopes.

[1]Fermionic Dy's magnetic moment is the largest of all elements, and bosonic Dy's magnetic moment is equal only to terbium's [2].

Standard spectroscopic records [2] had misrecorded by 21% the linewidth of the 401-nm state used for Er laser cooling [9]. Linewidth verification of the analogous transition in Dy (at 421 nm) is therefore justified, and we present a linewidth measurement that is consistent with previous measurements. Finally, we discuss the properties and relative merits of other optical transitions at 598 nm, 626 nm and 1001 nm that could also be used for laser cooling.

II. THE 741-NM TRANSITION

We discuss in this section an optical transition at 741 nm that could prove important for creating narrow-line Dy MOTs. Although the broad, blue 421-nm transition is highly effective for cooling Dy atoms from an atomic beam and in a MOT [10], the transition's Doppler limit of $\sim$1 mK is too high for directly loading an ODT. Because of its narrow linewidth, the red 741-nm transition provides a means to Doppler cool with a very-low-temperature limit. Our measurements indicate that this transition's recoil-limited temperature would be higher than its Doppler-limited temperature. Coupled with Dy's large magnetic moment, this narrow line might allow the observation of novel laser-cooling phenomena beyond that observed in the Er and Sr systems [8,11].

A. Experimental apparatus for measuring isotope shifts and hyperfine structure

The spectroscopic measurement for determining the isotope shifts and hyperfine structure employs a method of crossed excitation laser and atomic beam [12]. In a ultrahigh vacuum (UHV) chamber [10], thermal Dy atoms effused from a high-temperature oven working at 1275 °C. The atoms were collimated by a long differential pumping tube, which formed an atomic beam with a diameter of 5 mm and a diverging (half) angle of $\sim$0.02 rad. The beam entered a chamber with two pairs of optical viewports oriented orthogonally to the atomic beam.

A 5-mW, 741-nm laser beam [$1/e^2$ waist (radius) $\approx$2 mm] from an external cavity diode laser (ECDL) was directed through the UHV chamber via one pair of viewports. This laser has a mode-hop-free region of 20 GHz. Atomic fluorescence on the 741-nm line was collected through an orthogonal viewport by a 2-in. antireflection-coated achromatic lens pair with a

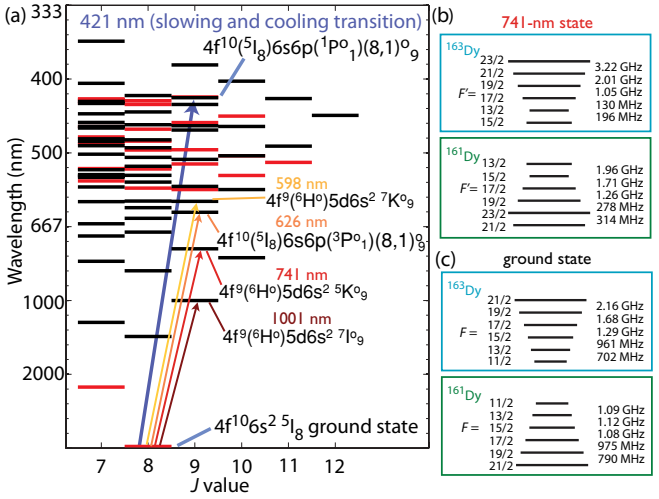

FIG. 1. (Color online) (a) Dy energy-level diagram with high J values [2]. The relevant laser cooling transitions between the even parity (red) ground state and the odd (black) excited states are marked with wavelengths and spectroscopic terms. Dy's five high-abundance isotopes have nuclear spin $I = 0$ for the bosons ^{164}Dy, ^{162}Dy, and ^{160}Dy and $I = 5/2$ for the fermions ^{163}Dy and ^{161}Dy. (b) Fermion hyperfine structure in the 741-nm state (not to scale) determined from measurements in Sec. II B. (c) Fermion ground-state hyperfine structure (not to scale) [3]. $F = J + I$, where J is the total electronic angular momentum.

magnification of 0.4×. This formed an image on the detection area (1-mm diameter) of a femtowatt photodetector (dc gain: 1×10^{10} V/W, bandwidth $\geqslant$750 Hz). The whole system was carefully shielded from stray light.

The direct output from the detector suffers from low signal-to-noise (SNR) ratio as a result of the oven's thermal radiation and the multiple scattering of 741-nm light from the windows and the chamber's inner walls. Averaging 512 times and adding an electronic bandpass filter (0.3 to 3 kHz) with

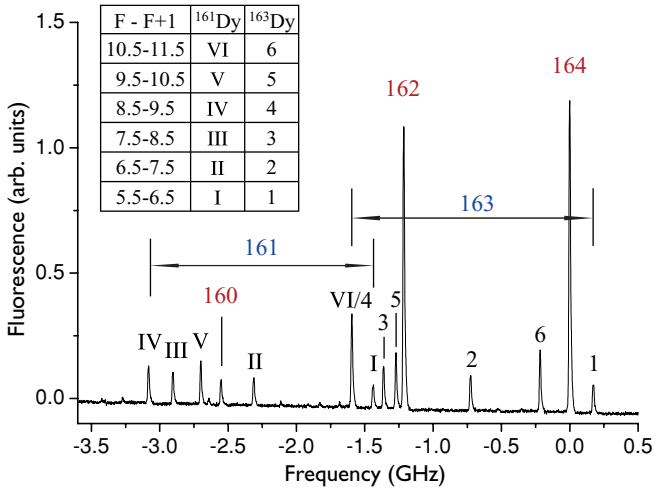

FIG. 2. (Color online) The 741-nm line spectrum for the five most abundant Dy isotopes. Bosonic isotope peaks are marked with mass numbers in red. Hyperfine peaks of fermionic isotopes (blue) are identified by the markers defined in the inset table. The VIth peak of ^{161}Dy and the 4th peak of ^{163}Dy overlap.

TABLE I. Values of hyperfine coefficients A and B (MHz) for the excited state (e) of the 741-nm transition in Dy including comparison with those of the ground state (g).

Coeff.	^{163}Dy$_{\text{theor}}$ [a]	^{163}Dy$_{\text{expt}}$	^{161}Dy$_{\text{expt}}$	$163_e/161_e$	$163_g/161_g$ [b]
A	142	142.91(3)	−102.09(2)	−1.3999(4)	−1.40026(4)
B	4000	4105(2)	3883(1)	1.0570(9)	1.05615(90)

[a]Reference [13].
[b]Reference [3].

a dc amplification of 10 improved the SNR to a sufficient level without artificially broadening the Doppler-limited resonances. With a laser scanning rate of 7 GHz/s and Doppler broadening of 15 MHz (measured in Sec. III), the ∼2-ms transit times of the spectral peaks were only somewhat slower than the detector's response time (200 μs). Nevertheless, all relative-peak-position data were sufficiently insensitive to this effect to render it negligible for the following analysis.

To measure the full spectrum of isotope shifts and hyperfine states, we scanned the ECDL using a piezoelectric transducer (PZT) that modulates its grating position. However, the free scan of the ECDL suffered from slightly nonlinear scanning of the PZT versus drive voltage. We reduced the nonlinearity by limiting the scan range and by scanning the PZT slowly to prevent inertial effects. To calibrate the frequency scan, we coupled the 741-nm light into a temperature-stabilized, 750-MHz, free-spectral-range (FSR) confocal cavity. Simultaneously recording the transmission of the confocal cavity with the fluorescence signal provided a frequency calibration as the ECDL was scanned. Cavity frequency intervals were calibrated by imprinting rf sidebands—which repeat every FSR interval—onto the cavity-coupled 741-nm light with a stable and calibrated rf frequency source. To correct for the nonlinearity of the scan, a calibration was performed by fitting a polynomial to the cavity spectrum. The maximum deviation throughout the scan due to a quadratic term was 3% of the linear term (the cubic term is negligible); we corrected the nonlinear effect up to quadratic order.

The calibrated spectrum after 512 averages is shown in Fig. 2. These data are sufficient to resolve and identify all $J \to J + 1$ ($F \to F + 1$) 741-nm transitions for the bosonic (fermionic) isotopes. Optical pumping is a negligible effect in this spectrum since the ∼10-μs transit time is much shorter than the transition lifetime (see Sec. II D).

B. Hyperfine structure

The position and ordering of ^{163}Dy's and ^{161}Dy's hyperfine peaks in the spectrum are determined by the ground and excited state's A and B coefficients.[2] Identification of the isotope and hyperfine transition peaks were found with guidance from the calculations in Ref. [13], and a least-squares-fitting routine extracted the experimental values of A and B (see Table I). Since this is a cycling $J \to J + 1$ transition, the strongest observed lines for the fermions are of the $F \to F + 1$ type;

[2]The A and B coefficients are defined in, e.g., Ref. [6].

TABLE II. Isotope shifts in the 741-nm and 457-nm transitions in Dy.

Isotope shifts	741 nm (MHz)	457 nm[a] (MHz)
^{164}Dy	0	0
^{163}Dy	−915(2)	660(3)
^{162}Dy	−1214(3)	971(2)
^{161}Dy	−2320(5)	1744(3)
^{160}Dy	−2552(5)	2020(3)

[a]Reference [16].

the much weaker [14] $F \rightarrow F$ transitions are visible as the small, unlabeled peaks in Fig. 2.

We note that for the excited states, the ratios of $A_e^{163}/A_e^{161} = -1.3999(4)$ and $B_e^{163}/B_e^{161} = 1.0570(9)$ are consistent with the analogous ratios for the ground state; there is no noticeable hyperfine anomaly for the 741-nm transition [15]. The ground-state hyperfine coefficients are $A = 162.754(2)$ and $B = 1152.869(40)$ for ^{163}Dy and $A = -116.231(2)$ and $B = 1091.577(50)$ for ^{161}Dy [3].

C. Isotope shifts

The measured isotope shifts (from ^{164}Dy to ^{160}Dy) for the 741-nm transition are listed in Table II, together with the isotope shifts for the 457-nm line. The 457-nm line has a purely electronic configuration, which makes it useful as a reference transition for creating the King plot [17] (Fig. 3). The fermionic isotope shifts are derived from the center of gravity of the hyperfine peaks, the positions of which were extracted from hyperfine structure fits. We could not obtain the isotope shift of ^{158}Dy and ^{156}Dy due to their low natural abundances and the weak strength of the 741-nm transition.

The isotope shift arises because of the differences in the masses and volumes of the nuclei of the isotopes and has the following form: $\delta f_{i,A} = E_A V_i + M_{i,B}$, where $\delta f_{i,A}$ is the isotope shift for the isotope pair i in the transition A. The

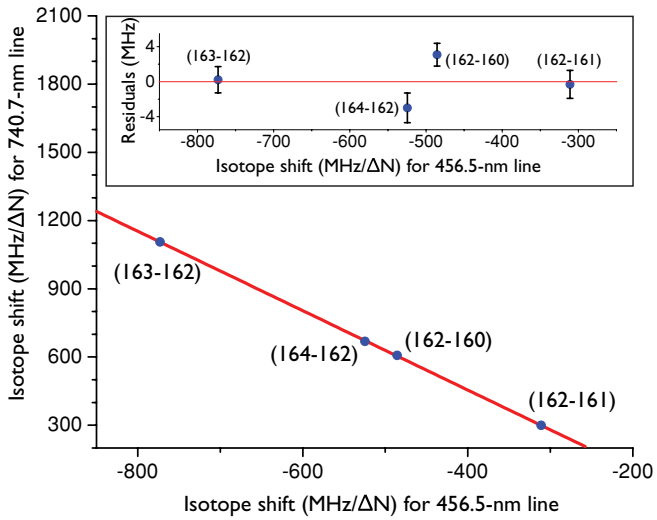

FIG. 3. (Color online) King plot of the isotope shifts in the 741-nm line vs isotope shifts in the 457-nm line. ΔN is the mass number difference between isotope pairs. Inset is the fit residual.

first term on the right-hand side is the contribution from the volume effects, which can be decomposed into the electronic field-shift parameter E_A and volume factors V_i. The mass term $M_{i,A}$ can be further deposed into the sum of normal mass shift (NMS) $M_{\mathrm{NMS},i,A}$ and specific mass shift (SMS) $M_{\mathrm{SMS},i,A}$. The NMS is directly proportional to the change of the reduced electron mass between the isotope pair, which can be analytically calculated [17]. The SMS describes the correlation between momenta of electrons and is determined by the intercept of the King plot.

For two different transitions A and B, the equation can be rewritten as

$$\delta f_{i,B} = \frac{E_B}{E_A}\delta f_{i,A} + M_{i,B} - \frac{E_B}{E_A}M_{i,A}. \quad (1)$$

The new equation indicates that the experimental data fall on a line with a slope of $\frac{E_B}{E_A}$ (King's plot). The intercept of the plot provides the relation of mass shifts between A and B transitions. With the independent knowledge of the NMS and SMS for transition A and the NMS for transition B, the value of SMS for transition B is determined.

We draw the King plot using the documented $4f^{10}6s^2(^5I_8) \rightarrow 4f^{10}6s6p(^7I_8)$ transition at 457 nm as the reference transition [16,18]. As discussed previously, the isotope shift includes the contribution from the mass term, which is related to the change of isotope mass, and the field shift, which is due to the finite possibility of electrons being inside the nucleus. Different electron configurations lead to different field shifts: From the fit of the isotope shifts of the 741-nm transition plotted against those values for 457 nm, the ratio of electronic field-shift parameter $E_{741}/E_{457} = -1.746(9)$ is determined based on the slope of the linear fit. The minus sign indicates the very different nature of two transitions: one is of $4f \rightarrow 5d$ type while the other is $6s \rightarrow 6p$.

The NMS values for the 457-nm and 741-nm transitions are $\delta\nu^{457}_{\mathrm{nms}164-162} = 27$ MHz and $\delta\nu^{741}_{\mathrm{nms}164-162} = 17$ MHz, respectively [17]. The SMS of the 457-nm transition is 7(8) MHz [16], which allows us to calculate the SMS for the 741-nm line: $\delta\nu^{741}_{\mathrm{sms}164-162} = 563(17)$ MHz, based on the intercept of the King plot. Such a large SMS is known to arise from the following effects: $4f$ electrons deeply buried inside the electron core, strong electron correlations, and $4f$ electrons coupling to each other before coupling to the outer $6s$ electrons [19]. A transition of type $6s \rightarrow 6p$ leaves the inner electrons little changed, while $4f \rightarrow 5d$ transitions lead to large changes in the inner-electron correlations. The large experimental value of the 741-nm transition SMS is consistent with the typical values for $4f \rightarrow 5d$ transitions [20].

D. Lifetime measurement

A direct lifetime measurement based on the fluorescence decay observed with the crossed-beam method is not possible because of large transit-time broadening relative to the natural decay time. (The UHV chamber limits observation path length to a few centimeters; the 500-m/s beam velocity causes the transition time to be comparable to the transition lifetime.) Therefore, we resorted to measuring the fluorescence scattered from relatively static atoms, that is, from the ∼1 mK atoms in

the MOT and in the magnetostatic trap (MT). We measure a consistent lifetime with both methods.

In the MOT method, we shined a retroreflected 5-mW, 741-nm excitation beam with a 3-mm waist onto a MOT generated on the 421-nm transition and recorded the decay of 741-nm scattered light after the 741-nm beam was extinguished. While the 741-nm excitation beam was on, the system established a steady-state population distribution among the 421-nm, 741-nm, and ground states. By switching on and off the 741-nm laser beam with a period of 250 μs, the atoms initially shelved in the 741-nm state will decay back to the ground state via the spontaneous emission of 741-nm photons. The small $1:10^5$ branching ratio of the 421-nm transition, measured in previous work [5,10], means that the Dy atom is effectively a three-level system during the 250-μs decay measurement: decay out of the three-level system from 421-nm state to the metastable states occurs on a much longer time scale, >2 ms. Solutions to the optical Bloch equations [21] for such a "V" system—two excited states coupled to a ground state via resonant 421-nm and 741-nm light—verify that the decay rate observed is equal to the decay rate of the bare 741-nm state.

An avalanche photodetector (APD) and collection lenses with a 741-nm narrow bandpass filter was used to detect the weak signal, which we averaged 10 752 times to obtain the data in Fig. 4(a). Note that the presence of 421-nm light or magnetic-field gradients do not affect the natural decay-rate measurement of the closed 741-nm transition for either this method or the following one.

In the MT method, we extinguished the 421-nm MOT light and captured the atoms in the magnetic quadrupole field of the now-extinguished MOT. We waited 5 s to allow the atoms to equilibrate in the MT [5] before shining a resonant retroreflected 741-nm beam of 5 mW power and 3-mm waist onto the trap. A single photon counter with collection lenses and a 741-nm bandpass filter recorded the very weak flux of 741-nm photons from the MT after the 741-nm excitation beam was extinguished [see Fig. 4(b)]. The long experimental run time necessary to measure a single decay limits the obtainable statistics.

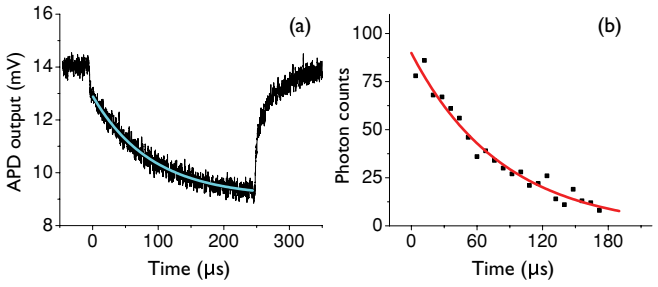

FIG. 4. (Color online) Measured decay of 741-nm fluorescence. (a) MOT method: Recorded 741-nm fluorescence signal from a Dy MOT by an APD averaged 10752 times. The blue line is an exponential fit to the fluorescent decay of the 741-nm level. The 741-nm excitation laser was turned off (on) at $t = 0$ ($t = 250$) μs. (b) MT method: Photon counting record of 741-nm fluorescence from atoms in a magnetic trap, accumulated 27 times, after the 741-nm excitation beam was extinguished at $t = 0$. The red line is an exponential fit to the decay.

TABLE III. Lifetime of the 741-nm excited state.

MOT method	MT method	Theory[a]
89.6(8) μs	84(14) μs	21 μs

[a]Reference [13].

Single exponential fits to the data in both methods derive lifetimes that are consistent with each other (see Table III). We note that the values are four times longer than the theoretical value reported in Ref. [13], and the measurement reported here may be used to refine Dy structure calculations [22]. With such a narrow linewidth—the weighted combination of the lifetime is 89.3(8) μs, resulting in a linewidth of 1.78(2) kHz—narrow-line cooling on the 741-nm transition is technically challenging for red-detuned narrow-line MOTs, since the laser linewidth should be comparably narrow [11]. However, a blue-detuned narrow-line MOT, which relies on the atoms' large magnetic dipole and has been demonstrated with Er [8], does not require a laser linewidth as narrow as the addressed atomic line; a narrow-line blue-detuned MOT on the 741-nm line seems feasible. While optical forces are not enough to support the atoms against gravity on these narrow lines, gravity is compensated by the magnetic force acting on the atom's large dipole moment in this blue-detuned narrow-line MOT.

III. THE 421-NM TRANSITION

Quantitative understanding of the population, dynamics, and cooling mechanisms [23] of the Dy MOT requires accurate knowledge of the 421-nm transition's linewidth. To ensure the use of the correct value of the 421-nm transition linewidth in laser-cooling calculations, we remeasured this linewidth using the crossed-beam method described earlier, though with a 421-nm beam derived from a frequency-doubled Ti:sapphire laser.

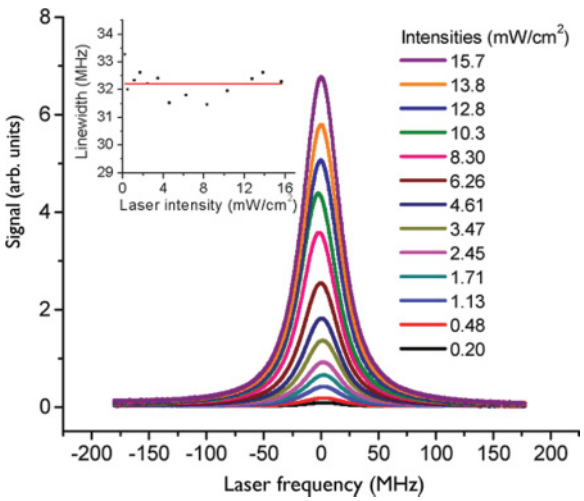

FIG. 5. (Color online) The photodetector signal as a function of 421-nm laser frequency, referenced to the line peak. The legend lists the laser intensities used in each measurement (highest laser intensity corresponds to highest signal). Each curve is averaged 64 times. Inset: Extrapolation of homogeneous linewidths to value at zero intensity.

TABLE IV. The 421-nm transition linewidth error budget.

Source	Uncertainty (MHz)
Extrapolation to zero intensity	0.13
Drift of laser during scans[a]	0.7
Laser linewidth	0.1
Rise time of detector	0.4

[a]Scan nonlinearity is negligible in transfer-cavity technique

To uniformly and stably scan the laser frequency, we employed the transfer cavity technique to lock the laser to a spectroscopic reference [10]. The optical transfer cavity is doubly resonant at 780 and 842 nm. The cavity itself was stabilized by locking a 780-nm ECDL to a hyperfine transition of the 780-nm $D2$ line in Rb before locking a resonance of the cavity to the stabilized ECDL. The Ti:sapphire laser, which generates the 842-nm beam, was then locked to this cavity. In order to scan the Ti:sapphire laser's frequency while the cavity remained locked to Rb, an electro-optical modulator driven by a microwave source generated tunable gigahertz-frequency sidebands on the 842-nm laser beam. By locking the sideband to the cavity, the carrier frequency can be stably scanned via tuning the microwave source. The 421-nm laser beam was obtained from a resonant lithium triborate (LBO) doubler. In the experiment, the laser frequency was scanned 400 MHz with a period of 1 s to ensure that the bandwidth of the PIN photodetector did not artificially broaden the transition. The fluorescence was collected via a pair of 2-in. achromatic doublets mounted outside an AR-coated UHV viewport. The electronic detector output was recorded on a fast digital oscilloscope and averaged 64 times.

The fluorescence versus frequency is shown in Fig. 5. The profile has the typical Voigt form due to the residual Doppler broadening of the atomic beam. Curves corresponding to different laser beam intensities possess differing linewidths due to power broadening. A global Voigt fit allows a deconvolution of the Doppler width from the transition linewidth by assuming a single Gaussian Doppler width and by accounting for the power broadening from the laser. The fitted value for the Doppler broadening is 14.8(6) MHz, which is consistent with the estimation of the residual Doppler broadening based on the geometry of the collimation tube and oven orifice.

At low intensities, the power broadening is linear as a function of laser intensity. A linear fit to the extracted linewidths provides the natural linewidth at the zero-intensity limit [9]. The extrapolated value for the natural linewidth of the 421-nm transition is 32.2(8) MHz. The uncertainty in the linewidth measurement arises from the error sources listed in Table IV. Among the errors, the largest source is the laser frequency drift from the imperfect transfer cavity lock. Unlike for Er [9], this measurement result is consistent with that listed in the standard tables, 33.1(17) MHz [2,24].

IV. ALTERNATIVE LASER-COOLING TRANSITIONS

Unlike the 421-nm line, the 598-, 626-, 741-, and 1001-nm lines are closed cycling transitions; laser cooling on them would obviate the need for repumping lasers or magnetic confinement in metastable states. While the 421-nm transition has been used to form the first Dy MOT [5] and the 741-nm transition—easily generated by a stabilized ECDL—is a good candidate for narrow-line cooling, the other three transitions might also be useful for laser cooling and trapping.

Table V summarizes these five laser cooling transitions: g is the Landé factor of the excited state; Γ is the transition decay rate; the linewidth is $\Delta\nu = \Gamma/2\pi$; and the excited state lifetime is $\tau = 1/\Gamma$. From these values, we can calculate some quantities of importance to laser cooling and trapping [6]. The saturation intensity $I_{\rm sat} \equiv \pi hc\Gamma/3\lambda^3$, for example, an estimate of the required MOT laser power; the capture velocity $v_{\rm cap} \equiv \Gamma\lambda/2\pi$ provides a measure of the velocity range within which atoms can be collected in a MOT; $T_{\rm Doppler} = \hbar\Gamma/2k_B$ is the Doppler cooling temperature limit; and $T_{\rm recoil} = \hbar^2k^2/mk_B$ is the temperature limit due to photon recoils.

The 1001-nm transition was considered as a candidate for narrow-line cooling because this is an intercombination transition which typically possesses narrow linewidth. We used the same experimental apparatus as in the 741-nm measurement—though a different ECDL laser—to find and measure the linewidth of the 1001-nm transition. However, we did not detect the line. Concurrently, theoretical calculations in Ref. [13] predicted the exceptionally small linewidth of 53 Hz, which explains our inability to detect the line with our current apparatus. This ultranarrow linewidth limits the transition's utility for a MOT, but along with the 741-nm line, the 1001-nm transition may be useful for resolved sideband cooling in an optical lattice [25–27]. This cooling technique may provide an alternative method [28] to evaporative cooling for the production of degenerate Dy gases.

TABLE V. Laser-cooling parameters for five cycling transitions in Dy; see text for parameter definitions.

Line	g	Γ	$\Delta\nu$	τ	$I_{\rm sat}$	$v_{\rm cap}$	$T_{\rm Doppler}$	$T_{\rm recoil}$
421 nm	1.22	$2.02 \times 10^8\ s^{-1}$ [a]	32.2 MHz	4.94 ns	56.4 mW/cm^2	14 m/s	774 μK	660 nK
598 nm	1.24	$7.7 \times 10^4\ s^{-1}$ [b]	12 kHz	13 μs	7.5 μW/cm^2	7.3 mm/s	294 nK	327 nK
626 nm	1.29	$8.5 \times 10^5\ s^{-1}$ [c]	135 kHz	1.2 μs	72 μW/cm^2	8.5 cm/s	3.2 μK	298 nK
741 nm	1.23	$1.12 \times 10^4\ s^{-1}$ [d]	1.78 kHz	89.3 μs	0.57 μW/cm^2	1.3 mm/s	42.7 nK	213 nK
1001 nm	1.32	$3.3 \times 10^2\ s^{-1}$ [e]	53 Hz	3 ms	6.9 nW/cm^2	0.05 mm/s	1.3 nK	116 nK

[a]Present work, 2.5% uncertainty.
[b]Reference [13], theory.
[c]Reference [2], experiment 5% uncertainty.
[d]Present work, 1% uncertainty.
[e]Reference [13], theory.

The 626-nm transition has a intermediate linewidth of 135 kHz, which could be used as the main laser cooling and trapping transition in a MOT while the atomic beam is Zeeman-slowed via the broad 421-nm transition. The benefit of such a combination [29] lies in the lower MOT temperature, since the 626-nm transition's Doppler limit is only 3.2 μK. A colder MOT facilitates subsequent ODT loading. However, this combination requires the use of a narrow-linewidth dye-based laser to obtain 626-nm light. We note that the large Landé g factor difference between the excited state (1.29) and ground state (1.24) suggests that intra-MOT sub-Doppler cooling [23,30] will not be as effective on this transition.

The linewidth of the 598-nm transition has yet to be measured, but the calculated value [13] indicates a linewidth of 12 kHz. This narrow linewidth would be optimal for conventional narrow-line cooling as performed in ultracold Sr experiments [11], for example, but again, the line must be generated with a dye-based laser. Its excited-state Landé g factor (1.24) is almost the same as its ground state's, which bodes well for effective intra-MOT sub-Doppler cooling.

V. SUMMARY

We measured the natural lifetime of the 741-nm line of Dy using a Dy MOT and magnetic trap; the weighted average is 89.3(8) μs. We predict that this closed cycling transition will be useful for the formation of a narrow-line MOT, which could cool Dy to the ultracold temperatures necessary for loading an optical dipole trap. The isotope shifts and hyperfine structure (A and B coefficients) were measured for all five high-abundance Dy isotopes, providing a spectral road map for the future narrow-line cooling of bosonic and fermionic Dy. In addition, we verified the linewidth of the 421-nm transition in Dy to be 32.2(8) MHz, a precautionary measure taken since the standard tables had listed the analogous transition in Er to be in error by 21%. Finally, we tabulated—based on up-to-date linewidth information—the laser-cooling properties of other attractive transitions in Dy.

ACKNOWLEDGMENTS

We acknowledge support from the NSF (PHY08-47469), AFOSR (FA9550-09-1-0079), and the Army Research Office MURI Award No. W911NF0910406.

[1] T. Lahaye, C. Menotti, L. Santos, M. Lewenstein, and T. Pfau, Rep. Prog. Phys. **72**, 126401 (2009); B. M. Fregoso, K. Sun, E. Fradkin, and B. L. Lev, New J. Phys. **11**, 103003 (2009); B. M. Fregoso and E. Fradkin, Phys. Rev. Lett. **103**, 205301 (2009); J. A. M. Huhtamäki, M. Takahashi, T. P. Simula, T. Mizushima, and K. Machida, Phys. Rev. A **81**, 063623 (2010).

[2] W. C. Martin, R. Zalubas, and L. Hagan, *Atomic Energy Levels—The Rare Earth Elements* (NSRDS-NBS, **60**, Washington, DC, 1978).

[3] W. J. Childs, Phys. Rev. A **2**, 1692 (1970).

[4] C. Hancox, S. Doret, M. Hummon, L. Luo, and J. Doyle, Nature (London) **431**, 281 (2004); B. Newman, N. Brahms, Y.-S. Au, C. Johnson, C. Connolly, J. M. Doyle, D. Kleppner, and T. J. Greytak (to be published).

[5] M. Lu, S.-H. Youn, and B. L. Lev, Phys. Rev. Lett. **104**, 063001 (2010).

[6] H. J. Metcalf and P. van der Straten, *Laser Cooling and Trapping* (Springer-Verlag, New York, 1999).

[7] S. Hensler, J. Werner, A. Griesmaier, P. O. Schmidt, A. Görlitz, T. Pfau, S. Giovanazzi, and K. Rzazewski, Appl. Phys. B **77**, 765 (2003).

[8] A. J. Berglund, J. L. Hanssen, and J. J. McClelland, Phys. Rev. Lett. **100**, 113002 (2008).

[9] J. J. McClelland, Phys. Rev. A **73**, 064502 (2006).

[10] S.-H. Youn, M. Lu, U. Ray, and B. L. Lev, Phys. Rev. A **82**, 043425 (2010).

[11] T. H. Loftus, T. Ido, A. D. Ludlow, M. M. Boyd, and J. Ye, Phys. Rev. Lett. **93**, 073003 (2004).

[12] W. Demtröder, *Laser Spectroscopy* (Springer-Verlag, Berlin, 2008).

[13] V. A. Dzuba and V. V. Flambaum, Phys. Rev. A **81**, 052515 (2010).

[14] I. I. Sobelman, *Atomic Spectra and Radiative Transitions* (Springer-Verlag, New York, 1992).

[15] D. L. Clark, M. E. Cage, and G. W. Greenlees, Phys. Lett. A **62**, 439 (1977).

[16] G. J. Zaal, W. Hogervorst, E. R. Eliel, K. A. H. van Leeuwen, and J. Blok, J. Phys. B **13**, 2185 (1980).

[17] D. Budker, D. F. Kimball, and D. P. DeMille, *Atomic Physics* (Oxford University Press, New York, 2008).

[18] N. Leefer, A. Cingöz, and D. Budker, Opt. Lett. **34**, 2548 (2008).

[19] R. D. Cowan, Nucl. Instrum. Methods **110**, 173 (1973).

[20] W.-G. Jin, T. Wakui, T. Endo, H. Uematsu, T. Minowa, and H. Karsuragawa, J. Phys. Soc. Jpn. **70**, 2316 (2001).

[21] C. Cohen-Tannoudji, J. Dupont-Roc, and G. Grynberg, *Atom-Photon Interactions: Basic Processes and Applications* (Wiley Science, New York, 1998).

[22] V. Dzuba (private communication).

[23] S.-H. Youn, M. Lu, and B. L. Lev, Phys. Rev. A **82**, 043403 (2010).

[24] J. J. Curry, E. A. Den Hartog, and J. E. Lawler, J. Opt. Soc. Am. B **14**, 2788 (1997).

[25] T. Ido and H. Katori, Phys. Rev. Lett. **91**, 053001 (2003).

[26] C. Grain, T. Nazarova, C. Degenhardt, F. Vogt, C. Lisdat, E. Tiemann, U. Sterr, and F. Riehle, Eur. Phys. J. D **42**, 317 (2007).

[27] V. A. Dzuba, V. V. Flambaum, and B. L. Lev, e-print arXiv:1011.4738 (2010).

[28] M. Olshanii and D. Weiss, Phys. Rev. Lett. **89**, 090404 (2002).

[29] T. Kuwamoto, K. Honda, Y. Takahashi, and T. Yabuzaki, Phys. Rev. A **60**, R745 (1999).

[30] A. J. Berglund, S. A. Lee, and J. J. McClelland, Phys. Rev. A **76**, 053418 (2007).